Elastic-Plastic Analyses of Cracked Straight and Curved Pipes under Bending

J. BROCHARD
CEA-CEN Saclay, Gif sur Yvette, France
S. C. CHHU
SOCOTEC Industrie, Montigny le Bretonneux, France
M. NEDELEC
CEA-CEN Fontenay-aux-Roses, Fontenay-aux-Roses, France

1 INTRODUCTION

Analytical tests were conducted, at CEA Saclay, on 100 mm diameter stainless steel straight pipes and elbows, containing through-wall circumferential cracks (Moulin et al. 1989). Those tubes were loaded in bending, without pressure, and at room temperature.

In this paper, we present 3D post-calculations of one straight pipe and one elbow, using the finite element technique, with CASTEM 2000 computer code. Even if the radius per thickness ratio is less than 10 (5.77 for the straight pipes and 6.17 for the pipe elbows), the cracked tubes were modelised with plate thin shell elements. Large displacements, but no large strain effects were taken into account. The engineering stress-strain curve (linear interpolation), with isotropic hardening and Von Mises criteria were considered. Considering that initiation was experimentally detected at 98 percent of the maximum moment, crack growth was not simulated. The objectives of these analyses is to check how accurate could be the numerical prediction of such cracked tubes using these calculation options.

2 DESCRIPTION OF CRACKED STRAIGHT PIPE TESTS

The experimental set-up is shown in fig. 1. The pipe was loaded in four-point bending, at quasi-static rates, under displacement control. The outer span was 1.9 m and the inner span 1.1 m.

The specimen was machined from a 4 inch schedule 160 pipe, without weld. Only 1.05 m center line of the pipe was machined on the outside diameter. Precise pipe dimensions are indicated in fig. 2. A through wall notch (31.67 percent of the circumference for pipe # 5) was machined into the pipe, and fatigue precracked prior conducting the experiment.

For pipe # 5, the final TWC length was 33.33 percent of the circumference (fig. 3). The material was an Z3CND 18-12 (316L) stainless steel. Tensile tests were conducted using round-bar specimens removed from the pipe moment arm, in the axial direction, after testing. Engineering stress-strain curve was considered in our analysis. Data are recorded in table 1.

Collected pipe data were: the applied load, the load-line displacement, crack mouth opening displacement, pipe rotations, ovalizations and also electrical measurements to detect crack initiation. Fig. 4 illustrates specific locations of the instrumentation.

3 CALCULATION OF STRAIGHT PIPE # 5

Due to symetry conditions, just one quarter of the cylinder was modelised using plate thin shell elements (Batoz et al., 1980). The 4 mm width notch was considered as a straight cut without thickness. The mesh was refined at the crack tip, and elements were arranged regulary within circular outlines, for an easier application of the virtual crack extension method to calculate the J-parameter (Parks, 1977) (fig. 5). From the elastic plastic calculation, rotations and ovalizations were determined and compared with experimental values. Figures 6 and 7 show the moment versus external rotation curves and moment versus internal rotation curves respectively. Fig. 8 shows the moment versus crack mouth opening displacement. Numerical and experimental results are in very good agreement. A stifferer behaviour is predicted numerically for high moment levels. The equivalent plastic strain exceeded the material ultimate tensile strain at 78 percent of the experimental maximum moment; however the calculation was continued, without divergence problem, because we had extrapolated the stress-strain curve by a constant stress value beyond the ultimate strengh. For the experimental maximum moment, we can notice an axial tearing at the crack tip, where plastic strains reached about 100 % (fig. 9). For the experimental initiation load, numerical and experimental values are recorded in table 2. For ovalizations, difference is less than 10 %. The load-line displacement was not in so good agreement, probably due to the influence of the loading frame compliance on the measurement.

Then, from the stress and strain fields, the J-parameter was calculated using the virtual crack extension method. On an other hand, from the experimental moment-rotation recordings, Moulin (1989) obtained an experimental J-value. Fig. 10 shows the comparison between the two J versus internal rotation curves. Numerical values are lower ($\simeq$ 25 %), but the experimental J evaluation is subjected to some scattering because plasticity spreaded on large parts of the component.

4 DESCRIPTION OF CRACKED PIPE ELBOW TESTS

For the cracked curved pipes, the experimental set-up is shown in fig. 11. A through-wall circumferential notch was machined into the elbows, and fatigue precracked prior testing. For curved pipes to be tested in the opening mode, the notch was machined in the intrados side. For tests in the closing mode, the notch was in the extrados side. Due to the manufacture process, thickness and material characteristics were not constant, but varied notably around the circumference.

Collected data were again: the applied load, the load-line displacement, crack mouth opening displacement, pipe rotations, ovalizations and electrical measurements to detect crack initiation.

5 CALCULATION OF PIPE ELBOW # 6

In a first step, it was choosen to calculate an elbow with the same crack size than the straigh pipe # 5 (33,33 percent of the circumference). It was pipe elbow # 6, whose TWC was on the extrados side, and which was tested in the closing mode. Like for the straight pipe, just one quarter of the cylinder was modelized with plate thin shell elements (fig. 14). Variations of the wall thickness around the circumference of the elbow was taking into account as well as possible, in the modelization, by means of 12 thickness zones (fig. 13 and table 3). For material tensile characteristics, just

2 zones were considered (fig. 12).

From the elastic plastic calculations, the moment-rotation recordings and moment-CMOD recordings were determined, and compared with the numerical data (fig. 15 and 16). Coincidence between numerical and experimental values is not as well as for the straight pipe; a stiffener elastic-plastic behaviour is predicted numerically. However, previous studies showed up to us that numerical prediction of such curved pipes is difficult, even if there is no defect.

Then, from the stress and strain fields, the J-parameter was calculated using the virtual crack extension method. Let us note that, in such a case, the virtual crack extension displacement field is not so easy to determine. For the straight pipe, a simple rotation around the pipe axis was used. But, here, each considered node must be rotated in its pipe section. However, procedures embedded in the computer code CASTEM 2000 proved to be efficient tools to carry out such kinds of numerical problems (Millard et al. 1987). Numerical and experimental J-values are compared in fig. 17: difference noted in the straight pipe results is erased by the stiffener behaviour.

CONCLUSION

Pipe # 5 calculation validated 3D thin shell analyses for prediction of the elastic plastic and fracture behaviour of stainless steel cracked straight pipes.

In case of carbon steel pipes, for which initiation would occur at low load level, several computations, with increasing crack angles, or a damage technique might be necessary to simulate the propagation.

For the cracked elbow, numerical prediction is not as well as for the straight pipe, but is acceptable regarding the notable variations of wall thickness and material characteristics.

REFERENCES

Moulin, D. et al. (1989). Experimental evaluation of J in cracked straight and curved pipes under bending, Transactions of the 10th SMIRT, Vol. G, pp. 323-326.

Batoz, J.L., Bathe, K.J. and Wingsho, L. (1980). A study of three node triangular plate bending element. International Journal for Numerical Methods in Engineering, Vol. 15, pp. 1771-1812.

Parks, D.M. (1977). The virtual crack extension method for nonlinear material behavior, Computer Methods in Applied Mechanics and Engineering.

Millard, A. et al. (1987). Non-linear algorithms solved with the help of the GIBIANE macro-language, Transactions of the 9th SMIRT, Vol. B, pp. 127-130.

Table 1. Engineering stress-strain tensile data for straight pipe # 5.

Stress (MPa)	115.0	144.0	168.0	192.0	217.0	254.5	284.8	315.1	345.4
Strain	0.0008	0.0011	0.0014	0.0020	0.0036	0.0125	0.0303	0.0481	0.0705

Table 1. Tensile data for pipe # 5 (continuation).

Stress (MPa)	372.7	403.0	433.3	463.6	493.9	512.1	515.1
Strain	0.1017	0.1285	0.1598	0.2044	0.2713	0.3383	0.4275

Table 2. Experimental and numerical values, for pipe # 5, at initiation moment.

Parameter	Expt. value	Calc. value	Difference
L.L displacement (mm)	8	5.75	30 %
External rotation (degrees)	7	6.16	12 %
Internal rotation (degrees)	5.1	4.54	11 %
Horizontal ovalizations (mm)	0.103	0.106	3 %
Vertical ovalizations (mm)	-0.096	-0.104	8 %

Table 3. Wall thickness values around the circumference, for elbow # 6.

Zone	1	2	3	4	5	6	7	8	9	10	11	12
Thickness (mm)	11.17	10.89	10.62	10.62	9.99	9.37	9.37	8.92	8.47	8.47	8.15	7.83

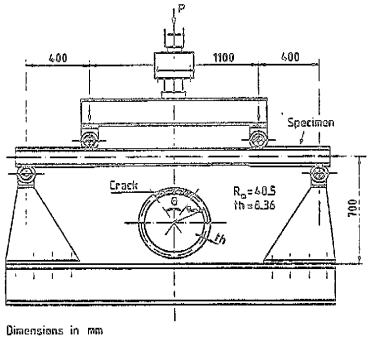

Fig. 1 - Experimental set-up for cracked straight pipes

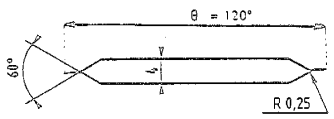

Fig. 3 - Through-wall notch geometry

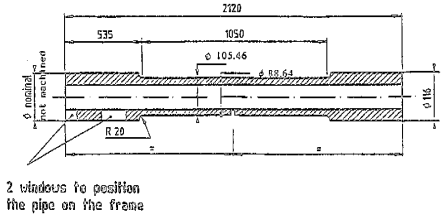

Fig. 2 - straight pipe geometry

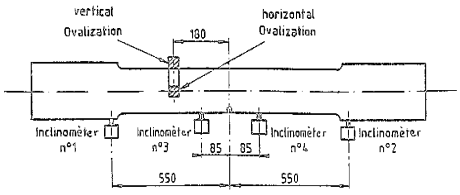

Fig. 4 - Instrumentation for rotation and ovalization measurements

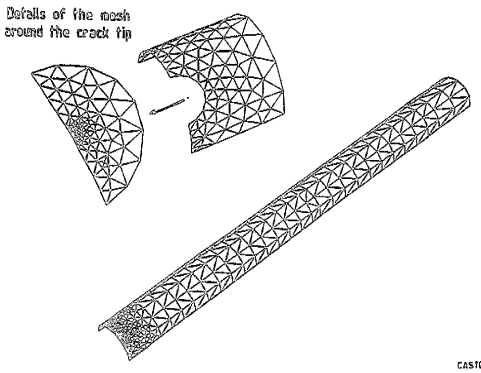

Fig. 5 - Cracked straight pipe mesh

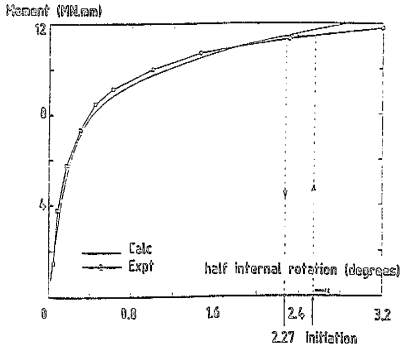

Fig. 7 - Moment versus internal rotation for expt # 5

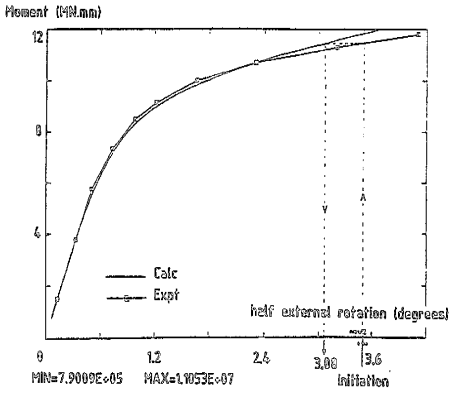

Fig. 6 - Moment versus external rotation for expt # 5

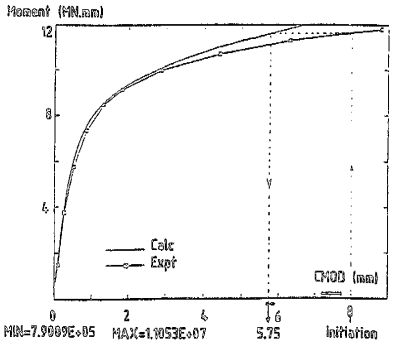

Fig. 8 - Moment versus CMOD for expt # 5

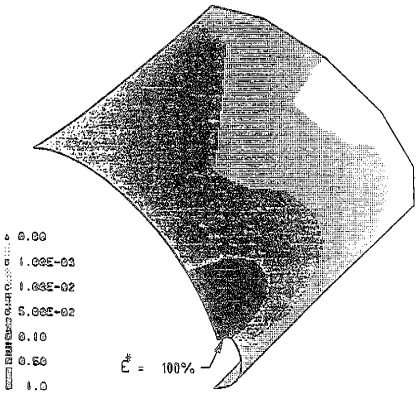

Fig. 9 - Equivalent strains at the maximum moment for expt # 5

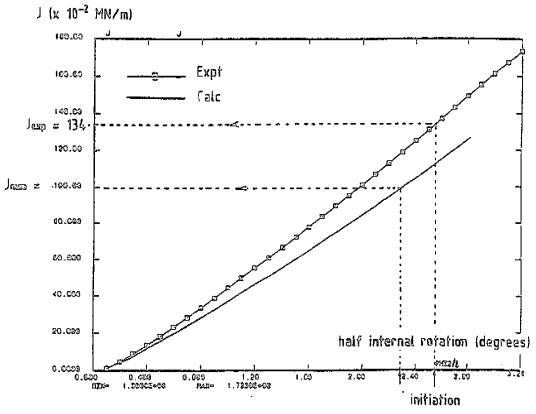

Fig. 10 - J versus internal rotation for expt # 5

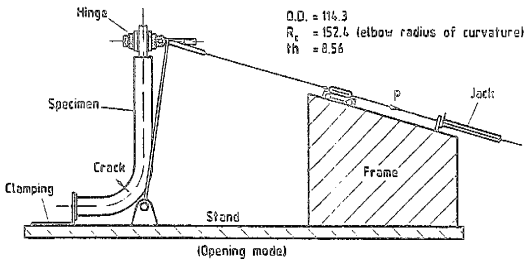

Fig. 11 - Experimental set-up for elbows

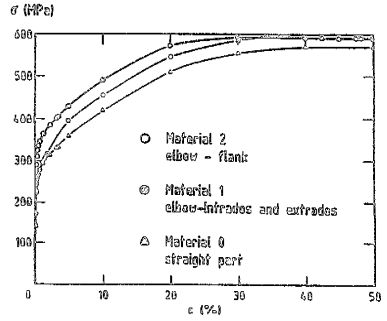

Fig. 12 - Stress-strain curves for the curved pipe

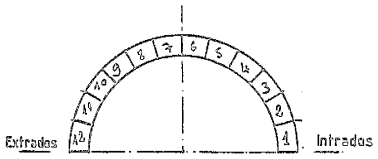

Fig. 13 - Different zones for elbow thickness

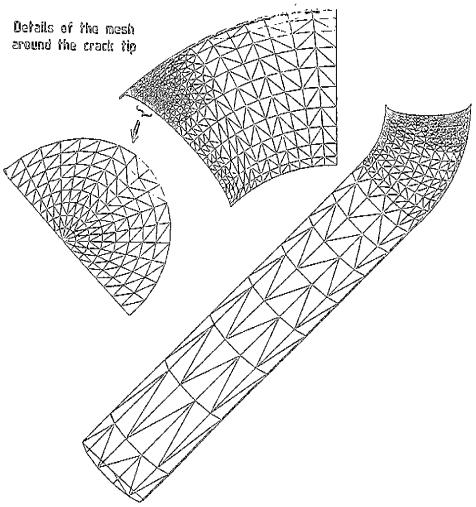

Fig. 14 - Cracked elbow mesh

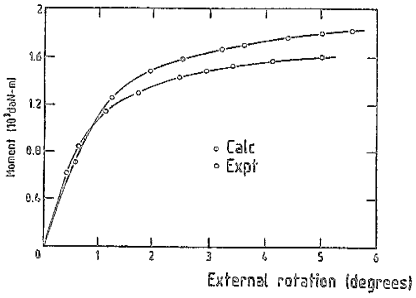

Fig. 15 - Moment versus external rotation for expt # 6

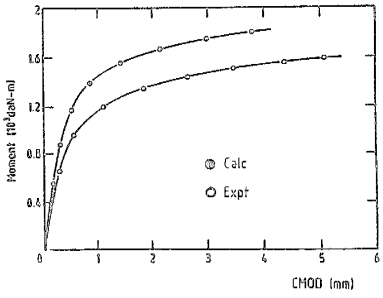

Fig. 16 - Moment versus CMOD for expt # 6

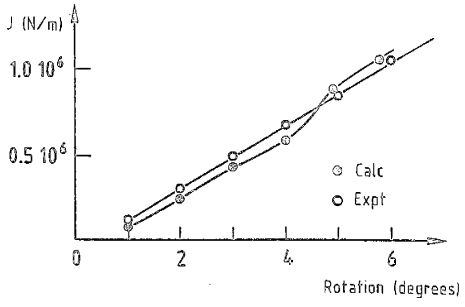

Fig. 17 - J versus rotation for expt # 6